Bent-Beam Electrothermal Actuators—Part II: Linear and Rotary Microengines

Jae-Sung Park, Larry L. Chu, Andrew D. Oliver, and Yogesh B. Gianchandani, *Member, IEEE*

Abstract—This paper reports on the use of bent-beam electrothermal actuators for the purpose of generating rotary and long-throw rectilinear displacements. The rotary displacements are achieved by orthogonally arranged pairs of cascaded actuators that are used to rotate a gear. Devices were fabricated using electroplated Ni, p^{++} Si, and polysilicon as structural materials. Displacements of 20–30 μm with loading forces > 150 μN at actuation voltages < 12 V and power dissipation < 300 mW could be achieved in the orthogonally arranged actuator pairs. A design that occupies < 1 mm^2 area is presented. Long-throw rectilinear displacements were achieved by inchworm mechanisms in which pairs of opposing actuators grip and shift a central shank that is cantilevered on a flexible suspension. A passive lock holds the displaced shank between pushes and when the power is off. This arrangement permits large output forces to be developed at large displacements, and requires zero standby power. Several designs were fabricated using electroplated Ni as the structural material. Forces > 200 μN at displacements > 100 μm were measured.   [624]

Index Terms—Inchworm, micromachining, micromotor, positioner, scanner, thermal actuator.

I. INTRODUCTION

BENT-BEAM suspensions may be used directly as electrothermal actuators, or as elements of larger actuation mechanisms that provide a vastly expanded scope of operation. In the preceding article [1] it was established that single beam actuators are capable of nonresonant, rectilinear displacements in the 10 μm range, and offer peak forces in the 1 mN range, whereas cascaded devices offer 2–4× higher displacement and about 10× lower peak forces. Devices with these characteristics can be used for applications such as operation of micro-relays, tuning of micromachined resonant sensors, tuning of micromachined capacitors, inductors, resonators, or other components for wireless communications, etc. However, there is also a need for micromechanisms that provide long throw rectilinear motion (≥ 100 μm) and rotary motion. These have been used in micromechanical discriminators for secure systems [3] as well
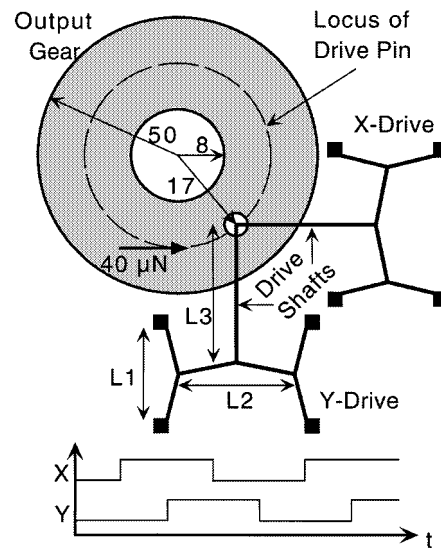
Fig. 1. Schematic (not to scale) of a rotary actuator based on orthogonal cascaded bent-beam elements for a gear of 50 μm radius.

as a variety of microoptical component such as scanners and switches [4]–[6].

This paper reports on rotary and rectilinear microengines that utilize the time-sequenced operation of bent-beam electrothermal actuators.[1] The rotary engines, which utilize two orthogonally placed actuators, are described in Section II. The rectilinear engines, which utilize two actuators and a mechanical lock in a grip-and-shift inchworm mechanism, are described in Section III.

II. ROTARY MICROENGINE

The rectilinear stroke of a microactuator can be converted into rotary motion of a gear by repeated tangential impact [7], [8] or by orthogonally placed linear actuators acting in tandem [3]. The latter alternative provides continuous application of force and can be easily implemented by an orthogonal arrangement of two electrothermal actuators. The time-sequenced operation of this mechanism provides the motion necessary to rotate the output gear. It may also be used as a general-purpose two–dimensional (2-D) positioner in the plane of the structure.

In order to meet the performance target for this effort, the rotary actuator must drive a 100-μm-diameter gear with a stall torque of at least 500 pN-m, using a drive voltage ≤ 12 V. As shown in Fig. 1, with the drive pin located 17 μm from the center of the gear, the target displacement for the actuators is about
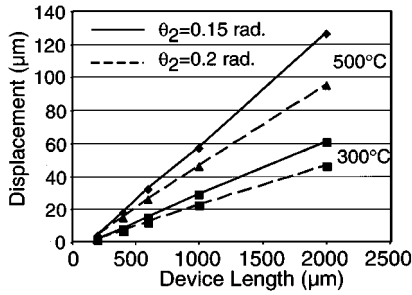
Fig. 2. Nonlinear FEA of an orthogonal pair of cascaded Si actuators with one axis actuated. Dimensions: $W1 = 6 \, \mu$m, $W2 = W3 = 4 \, \mu$m, $\theta1 = 0.1$ rad., $H = 4.5 \, \mu$m, and $L1 = L2 = L3$.

Fig. 3. FEA of orthogonal pairs, with 40 μN external loading force, and nonlinear expansion of Si. (a) Maximum average operating temperature that can be achieved before out-of-plane buckling occurs. (b) Lateral displacements that can be achieved before in-plane buckling occurs.

34 μm. The 500 pN-m stall torque requirement is satisfied if the output force at this displacement exceeds 29 μN. These specifications are difficult to meet with electrostatic actuators. Past reports indicate that when electrostatic forces are used, either the drive voltages are too high (≥ 30 V), the available forces are too low ($\leq 10 \, \mu$N), or both [8]–[11]. The low force can be compensated by lengthening the drive radius to increase the torque, but this constrains the mechanism to larger dimensions. In addition, some of the electrostatically driven mechanisms require intimate contact between the deflecting element and the substrate, raising the possibility of stiction related problems. Thus, the motivation for electrothermal actuation in this context is provided by both the higher available forces and the lower actuation voltages which permit the use of standard circuit interfaces.

The finite element analysis (FEA) of orthogonal pairs of identical cascaded actuators shows that a 30-μm stroke is achievable in Si with suspension lengths of $\approx 600 \, \mu$m at $< 500°$C (Fig. 2). This FEA model included both the X and Y actuators, and accounted for the loading of each upon the other (which is larger than 29 μN output load). Although shallower bending angles promise higher displacement, they have a greater propensity for out-of-plane buckling.

In designing the bent-beams, it should be noted that a longer suspension which offers large displacements is not always a better choice. A longer suspension will have higher mechanical compliance, and will consequently provide a smaller restoring force. At the completion of an actuation cycle (Fig. 1), the angular position of the drive gear and the location of the drive pin within its circular locus of motion will be determined by a balance between the restoring force and opposing friction. The design of the bent-beams must be such that the next rotation can be initiated from this position.

A. Buckling

In many cases, out-of-plane buckling can be the limiting factor for maximum displacement, output force, and drive temperature of an actuator. For cascaded structures and other complex shapes, FEA was used to examine stability. The buckling conditions of the structures were determined under an externally applied loading force of 40 μN, which included the maximum specified loading force of 29 μN as well as an 11 μN safety margin. The predictions for buckling temperature obtained by FEA were pessimistic because only one degree of freedom was specified. In reality, in-plane deflections that
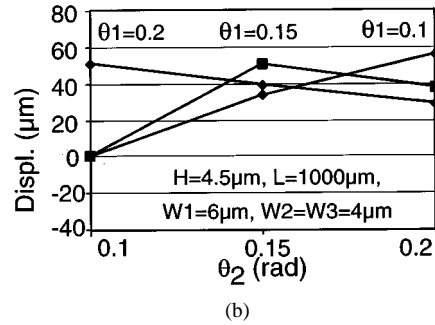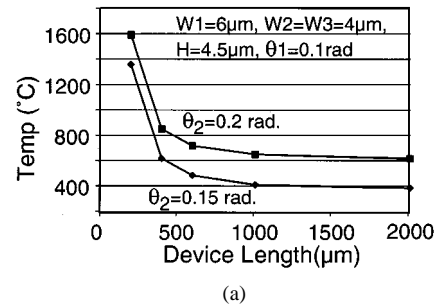
occur in normal operation of the device reduce the propensity for out-of-plane buckling. It is also helpful to evaluate the conditions for in-plane buckling. FEA predicts that when in-plane buckling occurs, the V-shape of the base unit in a cascaded device becomes inverted, rendering the device inoperational. Fig. 3(a) shows the temperature at which an actuator will buckle out-of-plane, whereas Fig. 3(b) shows the maximum lateral deflection that can be achieved before a cascaded actuator buckles in-plane. Bending angles of $\theta_1 = 0.1$ rad. and $\theta_2 = 0.2$ rad. provide the best compromise between large displacement and both in-plane and out-of-plane buckling. Process variations such as greater structural thickness or longitudinal corrugations in the structural material can help to further increase the out-of-plane buckling temperature.

B. Fabrication and Measurement Results

The operation of the orthogonal drive was first validated by fabricating it without the output gear, as shown in Fig. 4. Samples were fabricated in both electroplated Ni and p^{++} Si using abbreviated process sequences which provided a single structural layer. The loading of the gear on the actuator was emulated by a loading beam constrained by brackets at each end (Fig. 5). This beam was attached transversely to the drive shaft along each axis and/or at the location of the gear (Fig. 4).

A number of different designs were fabricated with dimensional variables as listed in Table I. The measured results are plotted in Fig. 6. For devices R3 and RJ3, there was no loading force applied, whereas for devices R5 and R6, loading force was applied only for displacement higher than a certain threshold, which was the displacement necessary for the loading beam to come into contact with its bracket constraint. Beyond this threshold, the loading force increased with displacement, which was measured using integrated verniers. The p^{++} Si devices
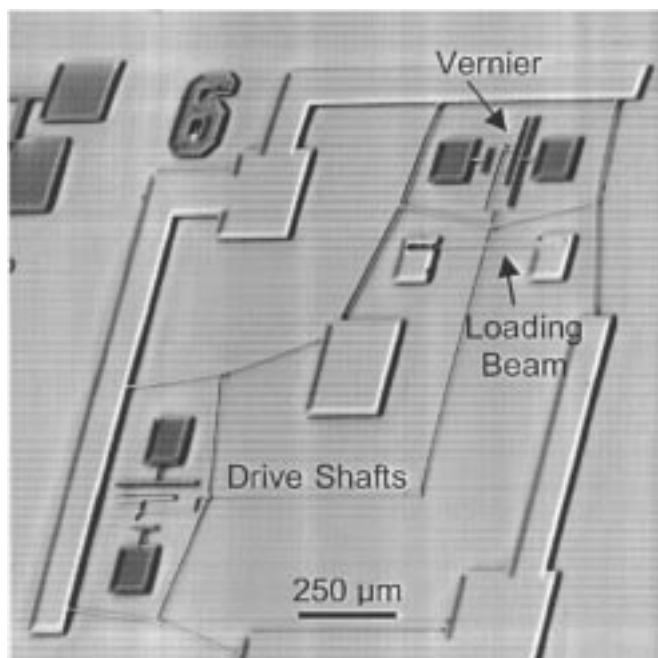
Fig. 4. SEM image of a orthogonal pair of cascaded actuators fabricated from p^{++} Si using the dissolved wafer process.
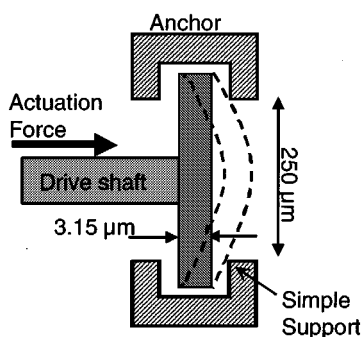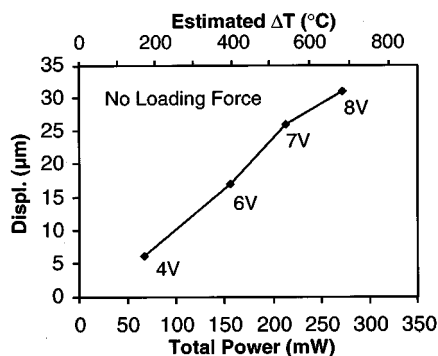

Fig. 5. Schematic of a loading beam used to measure output force available from an actuator.

with beam lengths of 500–1000 μm showed displacements of 20–30 μm when symmetrically driven at total power levels < 300 mW, and peak actuation voltages in the 6–8 V range. An electroplated Ni device with 500 μm beam length and 11 μm thickness provided 15 μm displacement at 0.8 V, and 450 mW. When a single axis is actuated, the drive pin at which the drive shafts meet experiences a backward displacement of about 1 μm along the complementary axis (Fig. 7). This displacement, which is predicted by FEA, can be explained as follows: when the X-drive shaft is bent by the actuation of the Y-drive, its projected length along the x-axis is reduced, causing a slight retraction of the drive pin in this direction. It is easily compensated by activating the complementary actuator.
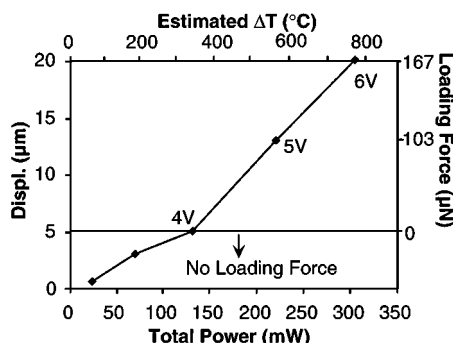
A modified version of the orthogonal drive that occupies < 1 mm^2 area is shown in Fig. 8. The X drive was comprised of two parallel primary bent-beams with $L_1 = 600$ μm, $W_1 = 3.7$ μm, $\theta_1 = 0.1$ rad. The secondary beam, which was attached to the apices of the primary beams at one end and anchored at the other end, had $L_2 = 600$ μm, $W_2 = 3.7$ μm, and $\theta_2 = 0.1$ rad. The Y drive was an ordinary cascaded device

Name	L	W1	W2	θ3	Load
R3	1000	4.3	2.3	0	none
R5	500	5.5	5.5	0	D
R6	500	5.2	3.2	0.2	Y
RJ3	500	5.7	6.7	0.2	none

(a)

(b)
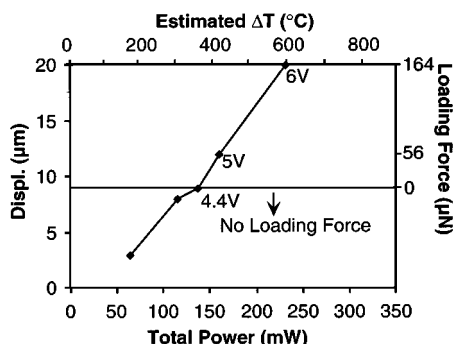
(c)

Fig. 6. (a)–(c) Displacement measurements of p^{++} Si rotary actuators R3, R5, and R6, respectively (Table I). In all cases the X and Y actuators were activated together.

with $L_1 = L_2 = 600$ μm, $W_1 = 5.7$ μm, $W_2 = 3.7$ μm, $\theta_1 = 0.1$ rad, and $\theta_2 = 0.2$ rad. The beams were 4.25 μm thick. The beams at both ends of the drive shaft and at the base of the secondary element in the Y-drive were narrowed to 1.7 μm width for a 40-μm-long segment in order to make

(a)

(b)

Fig. 7. Measured results of electroplated Ni rotary actuator RJ3 (Table I) with only one axis actuated. (a) Forward displacement of the actuated axis. (b) Small backward displacement along the orthogonal axis that can be easily compensated.

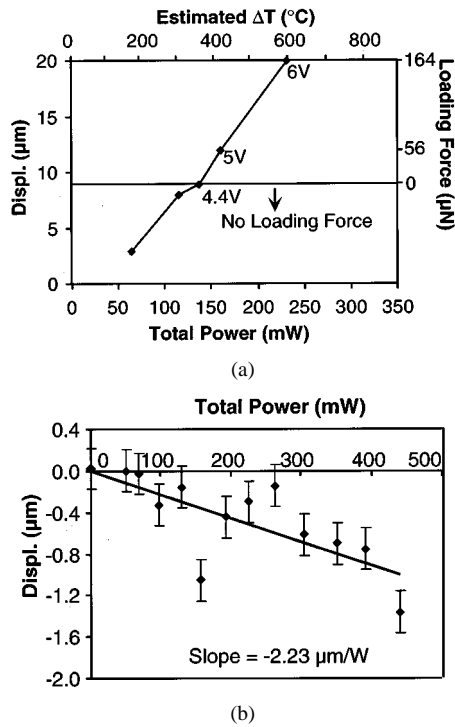the structure more compliant and reduce the load presented to the complementary drive. The segments of these beams that overlap the gears were 2.25 μm thick, while the gears were 2.5 μm thick. The device was fabricated using polysilicon as the structural material in the Sandia SUMMiT IV process.

The measured response of an isolated and unloaded instance of the cascaded polysilicon Y-drive is shown in Fig. 9. The peak displacement achieved was about 33.4 μm at 14.4 V and 375 mW. The operation of the microengine is shown in the optical micrographs of Fig. 10, which show the drive pin located in each quadrant as it rotated around the gear hub. The ON–OFF sequence of each drive is annotated in the figure. The peak voltage and current for the X-drive were 11.9 V and 17.9 mA, respectively; for the Y-drive, they were 9.6 V and 24.0 mA. A square wave signal which provided 50 ms in each quadrant was used to rotate the gear at 300 rpm. Measurements indicate that the -3 dB bandwidth for the displacement of the bent-beam electrothermal actuators is ≈ 700 Hz. This suggests that with proper timing and control, it may be possible to rotate the gears at about 15 000 rpm.

The devices were operated in air for > 15 min. The primary failure mode was the separation of the hub from the substrate, while secondary failure mode was the breaking of the pivot from the output gear. Both modes were probably related to the large forces applied by the electrothermal actuators; they are not commonly observed when electrostatic actuators, which provide much lower forces, are used to drive the same gears. Better control of the drive timing and larger feature sizes at the high stress points can alleviate this problem in future efforts. Another option is to use complaint microtransmissions, which can tailor the force–displacement relationship as required [12].
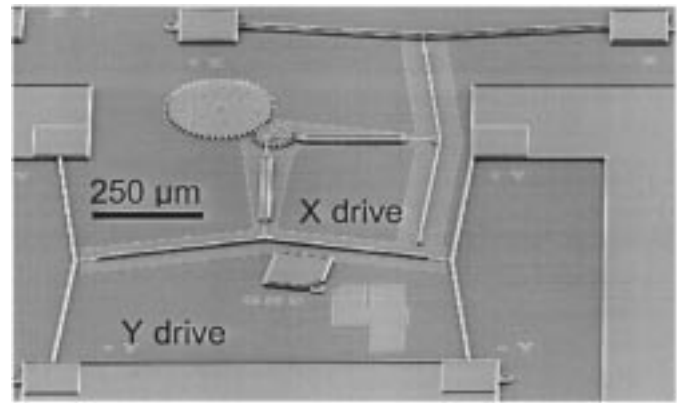
Fig. 8. An SEM image of a modified orthogonal-pair actuator fabricated in the Sandia SUMMiT process using polysilicon as the structural material.
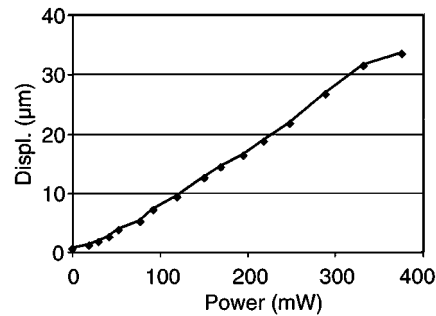
Fig. 9. Measured response of an isolated and unloaded Y-drive of the rotary actuator shown in Fig. 8. The maximum drive voltage used for this curve was 15 V.
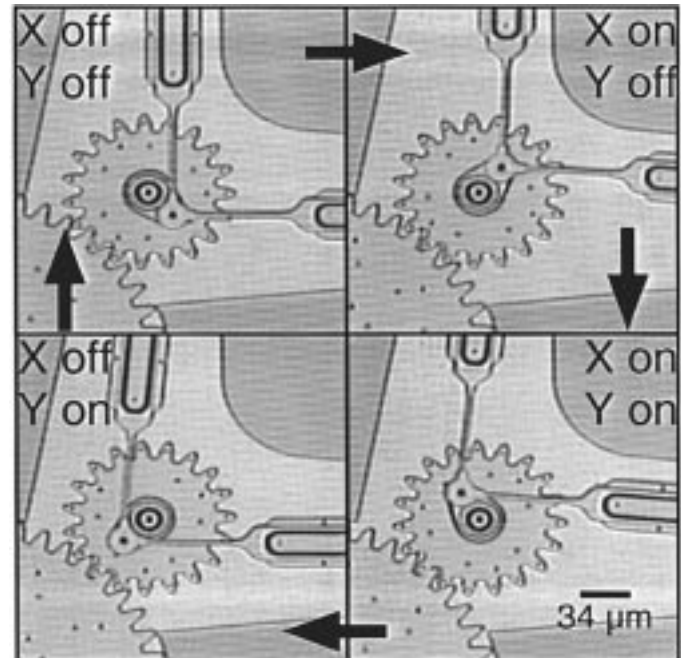
Fig. 10. Time sequenced operation of the rotary engine shown in Fig. 8.

III. INCHWORM TYPE MICROENGINE

One method to obtain long, linear displacements is to couple a rack to a rotary micromotor [3]. A second option is to extend the
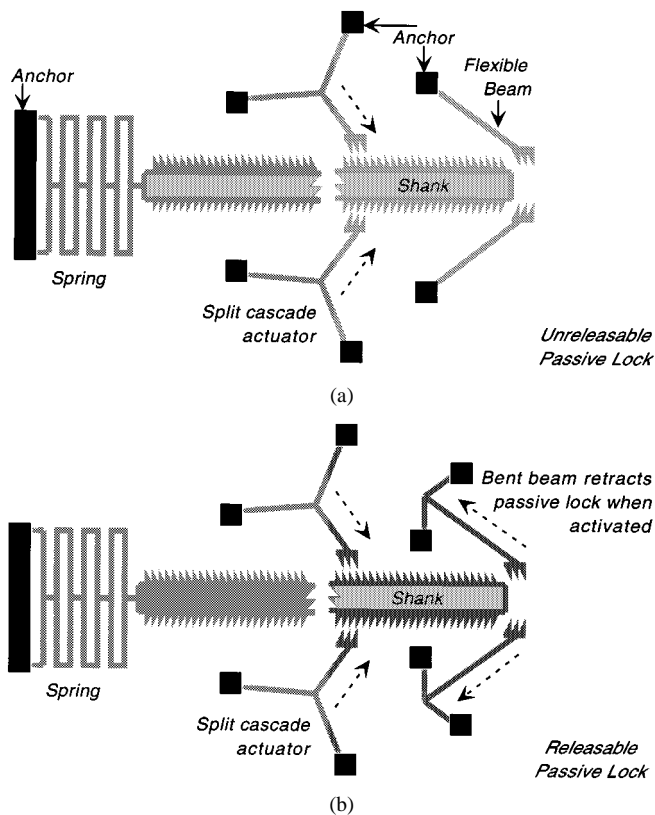
Fig. 11. (a) An inchworm actuator with passive lock that will prevent the pull-back of the shank when power to the actuator is turned off. (b) An inchworm with a retractable passive lock.

TABLE II
MEASUREMENT RESULTS OF ELECTROPLATED NI INCHWORMS LISTING DEVICE THICKNESS, PEAK DISPLACEMENT ACHIEVED, CALCULATED STIFFNESS OF THE SPRING AT THE BASE OF THE SHANK, AND ACTUATION METHOD (FOR WHICH $P = $ Voltage PULSE)

Device Type	Thick-ness (μm)	**Displ.** **(μm)**	K_{sp} (N/m)	Actuation Method
I11	9.0	**40**	0.51	DC: 1V
I33	14.0	**56**	0.895	P: 24 ms, 0.8V
I100	8.4	**32**	5.33	DC: 1V
IL1	11.0	**104**	1.96	P: 24 ms, 1.2V
IL4	9.8	**48**	1.73	P: 38 ms, 1.2V

concept of cascaded actuators to a distributed, web-like arrangement [13]. A third option is to accumulate short, linear displacements in the manner of an inchworm. Generally, two or more actuators are operated with a phase relationship that permits them to grip and shift a common slider along a fixed path. A single actuator may also provide this functionality if the slider, which is often spring-loaded, is restrained in some manner so that it does not retract between actuation cycles (pushes). Inchworms are widely used in centimeter-scale actuators, and have also been used for micromachined devices [14]–[19]. As with rotary actuators, when electrostatic drives are used, a compromise must be established between actuation voltages and output forces. The compromise can be partially ameliorated by increasing the drive capacitance using densely packed or taller electrodes, but it is difficult to exceed 100 μN with a 12-V bias. Since the output force determines the maximum deformation of the spring suspension to which the slider is attached, it also determines the maximum displacement. In order to obtain large displacements at low actuation voltages, one option is to not attach the slider to a spring suspension, which allows the mechanism to operate like the linear equivalent of an impact-driven motor [20], [21]. Another option is to explore the use of actuators that can provide larger forces.

In implementing the inchworm mechanism, pairs of opposing bent-beam actuators are pulsed to grip and shift a central shank, which is cantilevered on a flexible suspension (Fig. 11). The sidewall of the shank and the mating surfaces of the actuators are corrugated to reduce their reliance on friction to hold the displacement against large forces. The actuators effectively work

as a *split cascade*: when actuated, the individual actuators move forward until they touch the shank, at which point they effectively form a single actuator with an additional level of cascading. Another pair of opposing actuators, located at a different point along the shank, can be actively operated out of phase with the first to provide complementary motion. Alternatively, the second pair can serve as a passive lock that prevents the shank from being pulled back once it has been displaced. The concept of the passive lock is illustrated in Fig. 11(a): cantilevers placed at an angle lateral to the shank come into contact with it as the shank advances. The angle of their placement and the design of the corrugated mating surfaces is such that they offer little resistance to a forward displacement of the shank, which tends to disengage them from the teeth along its sides. Conversely, a reverse displacement of the shank tends to engage the intermeshed teeth, preventing it from being pulled back. The cantilevers may be optionally attached to actuators so that they may be retracted, as shown in Fig. 11(b). This results in tremendous power savings when a displacement must be held for extended time intervals. The incremental displacement of the shank is governed by the pitch of the corrugation on the shank and the face of the lock. The maximum displacement of the shank is reached when the pull-back force from the extension of the spring and the drag from the locking mechanism match the output force from the active pair of actuators.

A. Fabrication and Measurement Results

A number of different inchworms were designed and fabricated using a single structural layer of electroplated Ni. Preliminary tests were performed on five designs listed in Table II. Three of these, including I11, I33, and IL1 are shown in Figs. 12 and 13. Not shown are I100, which is similar to I33 but has a different spring, and IL4, which is similar to IL1 but has 40% longer beams, and releasable locks. Designs I11, I33, and I100 use pairs of simple actuators that effectively have a one-level cascade when they touch the shank, whereas designs IL1 and IL4 have a two-level cascade after they touch the shank. Designs I11 and IL4 have releasable passive locks, whereas the other have unreleasable ones.

The preliminary measurement results are summarized in Table II. Locked displacements of up to 104 μm were achieved using dc (≤ 1 V, 250 mA) or pulsed (≤ 1.2 V, ≤ 600 mA) actuation. The best pulse widths were empirically found to be in the 20–40 ms range. Each pulse advanced the shank by an integral multiple of 8 μm, which was the pitch of the corrugation along the sides of the shank. As shown in a close-up
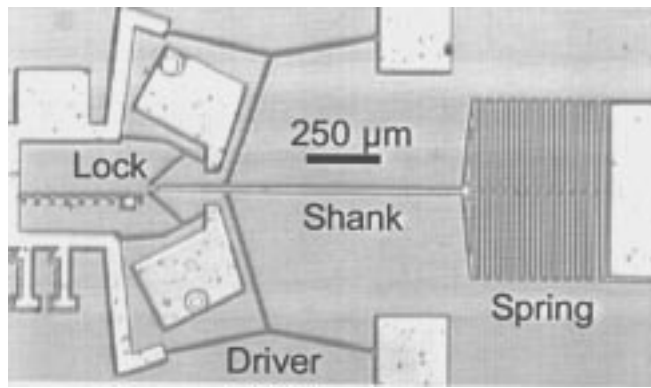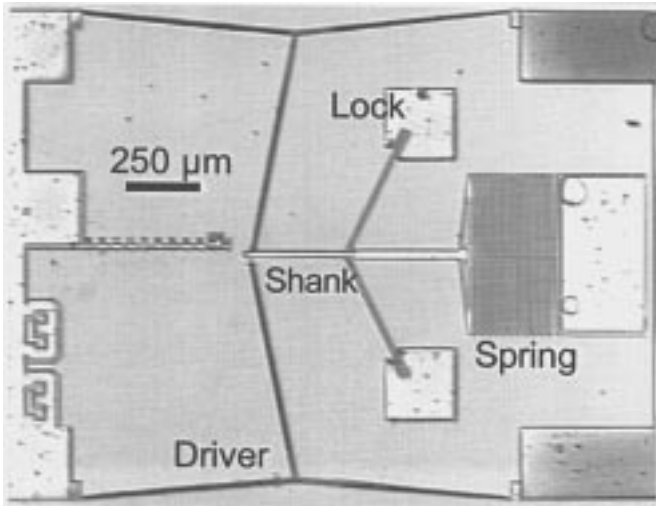
Fig. 12.   Optical micrographs of inchworms (a) I11 and (b) I33.

in Fig. 13, the lock holds the displacement when the power is turned off and the actuator is retracted.

The stiffness of the spring located at the base of each inchworm shank can be estimated from measured dimensional parameters by the formula:

$$K_{sp} = \frac{192 E I_s}{N L_s^3}$$

where

E Young's modulus of the electroplated Ni, estimated to be 150 GPa;

I_s moment of inertia of the spring beam, which is a half loop;

L_s length of the half loop;

N total number of half loops present.

This formula assumes fixed boundary conditions at the location of the fold in each loop, which matches observations of fabricated springs. Using this, the peak forces generated in devices I100 and IL1 were calculated as 171 and 204 μN, respectively (Table II). In reality, the maximum displacement achievable by the inchworm is limited not only by spring stiffness, but also by out-of-plane deformation of the actuators or the shank. These are caused by stress gradients in the structural material and by forcing together the sloping sidewalls of the shank and the mating surfaces of the actuators. These problems can be
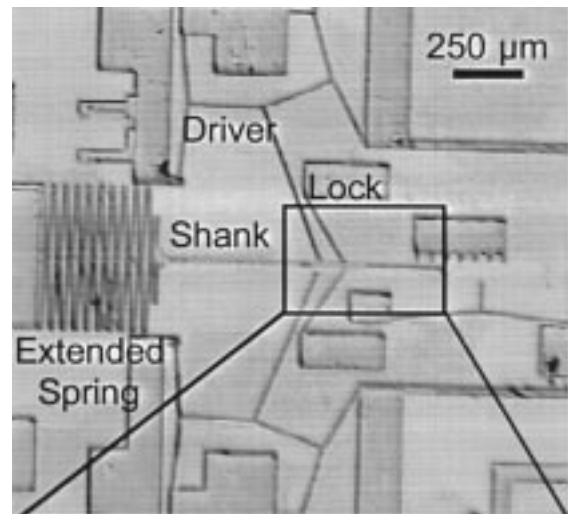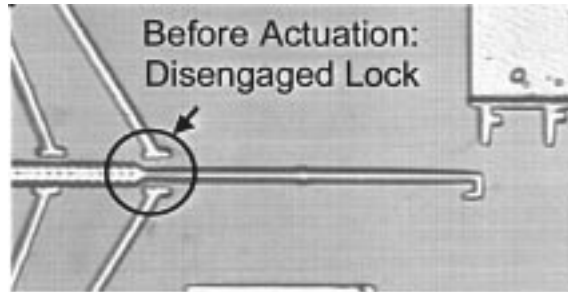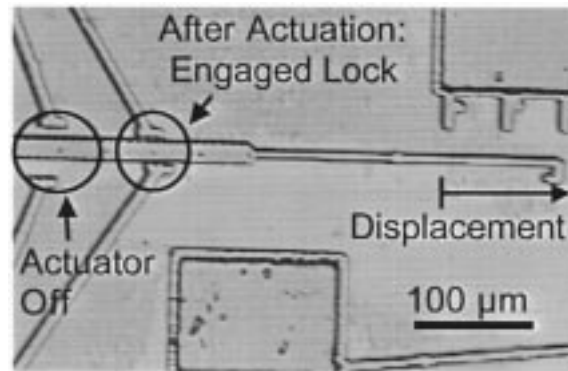
Fig. 13.   (a) Optical micrographs showing a locked displacement of 104 μm in inchworm IL1, (b) close-up images of the shank before actuation (lower left), and (c) after actuation.

solved by an improved fabrication process, which would result in peak output forces and displacements that are greater than the measurements listed in Table II. Another option is to add out-of-plane constraints using an additional structural layer.

IV. CONCLUSION

This effort has explored microengines based on bent-beam suspensions for the purpose of generating rotary and rectilinear displacements. Several different structural materials were evaluated, including electroplated Ni, bulk micromachined p^{++} Si, and surface micromachined polysilicon. Orthogonally placed pairs of cascaded thermal actuators which essentially formed

2-D positioners were applied to rotary drives. Structures fabricated from p^{++} Si with 500–1000 μm beam lengths and 6.5 μm thickness showed 20–30 μm diagonal displacement with $> 150 \mu$N loading at actuation levels of 6–8 V, and 250–300 mW. An electroplated Ni structure with 500 μm beam lengths and 11 μm thickness provided 15 μm displacement at 0.8 V, 450 mW. A modified rotary engine that occupied < 1 mm^2 area was formed by dropping one of the primary beams in the orthogonal pair of cascaded actuators. It was fabricated using surface micromachined polysilicon with beams of 600 μm length and 4.25 μm thickness, and used to drive a gear with actuation voltages below 12 V.

Opposing pairs of simple and cascaded actuators were applied to inchworms. Several designs were fabricated with electroplated Ni, and tested with DC and pulsed actuation schemes. Devices with 500–1500 μm beam lengths and 8–14 μm thickness provided displacements up to 104 μm against estimated loading forces up to 204 μN. Passive locks allowed the standby power to be reduced to zero.

Overall, these efforts have demonstrated that bent-beam electro-thermal actuators can be used to generate nonresonant displacements and forces that exceed those commonly available from electrostatic actuators. Both rotary and rectilinear engines can be easily designed and fabricated by silicon compatible lithography based micromachining techniques. Since the drive voltages are ≤ 12V and the power consumption is a few hundred milliwatts, standard electronic interfaces may be used to drive these actuators, making them suitable for a variety of applications.

ACKNOWLEDGMENT

REFERENCES

[1] L. Que, J.-S. Park, and Y. B. Gianchandani, "Bent-beam electrothermal actuators -I: single beam and cascaded devices," J. Microelectromech. Syst., vol. 10, pp. 247–254, June 2001, submitted for publication.

[2] J.-S. Park, L. L. Chu, E. Siwapornsathain, A. D. Oliver, and Y. Gianchandani, "Long throw and rotary output electro-thermal actuators based on bent-beam suspensions," in *Proc. IEEE International Conference on Micro Electro Mechanical Systems (MEMS00)*, Miyazaki, Japan, Jan. 2000, pp. 680–685.

[3] M. S. Rodgers and J. J. Sniegowski, "Five-level polysilicon surface micromachining technology: application to complex micromechanical systems," in *Solid-State Sensor & Actuator Workshop (Hilton Head)*, June 1998, pp. 144–149.

[4] E. J. Garcia, "Micro-flex mirror and instability actuation technique," in *Proc. IEEE Conf. on Micro Electro Mechanical Systems*, Heidelberg, Jan. 1998, pp. 470–5.

[5] A. A. Yasseen, J. N. Mitchell, D. A. Smith, and M. Mehregany, "High aspect ratio rotary polygon micromotor scanners," *Sensors Actuators*, vol. A77, no. 1, pp. 73–79, Sept. 1999.

[6] A. A. Yasseen, T. S. Mitchell, D. A. Smith, and M. Mehregany, "A rotary electrostatic micromirror 1×8 optical switch," in *Proc. IEEE Conf. on Micro Electro Mechanical Systems*, Heidelberg, Germany, Jan. 1998, pp. 116–120.

[7] A. P. Lee and A. P. Pisano, "Polysilicon angular vibromotors," *J. Microelectromech. Syst.*, vol. 1, pp. 70–76, June 1992.

[8] M. Okyar, X.-Q. Sun, and W. N. Carr, "Thermally excited inchworm actuators and stepwise micromotors: analysis and fabrication," *Proc. SPIE*, vol. 3224, pp. 372–379, 1997.

[9] K. C. Stark, M. Mehregany, and S. M. Phillips, "Mechanical coupling and direct torque measurement of outer-rotor polysilicon micromotors," in *Proc. IEEE Workshop on Micro Electro Mechanical Systems (MEMS '97)*, Nagoya, Japan, Jan. 1997, pp. 221–226.

[10] D. A. Horsley, M. B. Cohn, A. Singh, R. Horowitz, and A. P. Pisano, "Design and fabrication of an angular microactuator for magnetic disk drives," *J. Microelectromech. Syst.*, vol. 7, pp. 141–148, June 1998.

[11] P. Minotti, P. Langlet, G. Bourbon, and T. Masuzawa, "Design and characterization of high-torque/low-speed silicon based electrostatic micromotors using stator/rotor contact interactions," *Japanese J. Appl. Phys.*, vol. 37, no. 3B, pp. L 359–361, Mar. 1998.

[12] L. Chu, J. Hetrick, and Y. Gianchandani, "Electro-thermal actuators using optimized compliant microtransmissions as rectilinear motion amplifiers," in *Proc. Solid-State Sensors and Actuators Workshop (Hilton Head '00)*, Hilton Head, SC, June 2000.

[13] K. Minami, S. Kawamura, and M. Esashi, "Fabrication of distributed electrostatic micro actuator (DEMA)," *J. Microelectromechan. Syst.*, vol. 2, pp. 121–127, Sept. 1993.

[14] N. R. Tas, A. H. Sonnenberg, A. F. M. Sander, and M. C. Elwenspoek, "Surface micromachined linear electrostatic stepper motor," in *Proc. IEEE Workshop on Micro Electro Mechanical Systems (MEMS '97)*, Nagoya, Japan, Jan. 1997, pp. 215–220.

[15] N. Tas, J. Wissink, L. Sander, T. Lammerink, and M. Elwenspoek, "The shuffle motor: a high force, high precision linear electrostatic stepper motor," in *Proc. IEEE International Conference on Solid-State Sensors and Actuators (Transducers '99)*, Chicago, IL, June 1997, pp. 777–780.

[16] M. Baltzer, T. Kraus, and E. Obermeier, "A linear stepping actuator in surface micromachining technology for low voltages and large displacements," in *Proc. IEEE International Conference on Solid-State Sensors and Actuators (Transducers '99)*, Chicago, IL, June 1997, pp. 781–784.

[17] R. Yeh, S. Hollar, and K. S. J. Pister, "Single mask, large force, and large displacement electrostatic linear inchworm motors," in *Proc. IEEE Int. Conf. on Micro Electro Mechanical Systems (MEMS '01)*, Interlaken, Switzerland, Jan. 2001, pp. 260–264.

[18] T. Akiyama and K. Shono, "Controlled stepwise motion in polysilicon actuators," *J. Microelectromech. Syst.*, vol. 2, pp. 106–110, Sept. 1993.

[19] P. Langlet, D. Collard, T. Akiyama, and H. Fujita, "A quantitative analysis of scratch drive actuation for integrated X/Y motion system," in *Proc. IEEE Int. Conf. on Solid-State Sensors and Actuators (Transducers' 97)*, Chicago, IL, June 1997, pp. 773–776.

[20] M.-H. Kiang, O. Solgaard, K. Y. Lau, and R. S. Muller, "Electrostatic combdrive-actuated micromirrors for laser-beam scanning and positioning," *J. Microelectromech. Syst.*, vol. 7, pp. 27–37, Mar. 1998.

[21] M. Pai and N. C. Tien, "Current-controlled bi-directional electrothermally actuated vibromotor," in *Proc. IEEE Int. Conf. on Solid-State Sensors and Actuators (Transducers '99)*, Sendai, Japan, June 1999, pp. 1764–7.

Jae-Sung Park received the B.S. degree from Pohang University of Science and Technology and the M.S. degree from Seoul National University, Korea, in 1995 and 1997, respectively, both in mechanical engineering. He is currently pursuing the Ph.D. degree in mechanical engineering Department at the University of Wisconsin, Madison.

As a Masters student, he was involved in developing optical probe measurement tools. Since 1997, his research has focused on microelectromechanical systems (MEMS) design and fabrication, with emphasis on microactuators and pressure sensors.

Larry L. Chu received the B.S. and M.S. degrees from the University of Wisconsin–Madison in 1998 and 2001, respectively, both in electrical and computer engineering. He is currently pursuing the Ph.D. degree in the same department.

In 1997, he helped to develop an undergraduate level fiber optics communications instructional laboratory. From 1998 to present, he holds a research assistantship with the Microsystems Lab at the University of Wisconsin–Madison. His research focuses on the microelectromechanical systems (MEMS) technology and its applications to material characterization, optical communication, and micropositioning.

Andrew D. Oliver received the B.S.E.E. degree from Iowa State University, Ames, in 1991 and the M.S.E.E. and Ph.D. degrees in electrical engineering from the University of Michigan, Ann Arbor, in 1993 and 1997, respectively. In 1997, he joined the Electromechanical Engineering Department at Sandia National Laboratories, Albuquerque, NM, where he is a Senior Member of the Technical Staff. His research interests include: the design and fabrication of silicon micromachines (both surface and bulk), the packaging of surface micromachines, and uncooled infrared detectors.

Yogesh B. Gianchandani (S'83-M'95) received the B.S. degree from University of California, Irvine, the M.S. degree from the University of California, Los Angeles, and the Ph.D. degree from the University of Michigan, Ann Arbor, all in electrical engineering, in 1984, 1986, and 1994, respectively.

From 1985 to 1988, he was with Xerox Corporation and from 1988 to 1989, he was with Microchip Technology, Inc., working in the area of integrated circuit design. From 1994 to August 1997, he was a Research Fellow in the Center for Integrated Sensors and Circuits at the University of Michigan, Ann Arbor. Since then he has been with the University of Wisconsin, Madison, as an Assistant Professor in the Department of Electrical and Computer Engineering. His research interests include all aspects of design, fabrication, and packaging of micromachined sensors and actuators and their interface circuits.

Dr. Gianchandani received the National Science Foundation Career Award in 2000. He serves on the editorial boards of two technical journals, and on the steering committee for the IEEE International Conference on Microelectromechanical Systems (MEMS).